Effect of O_3 on the atmospheric temperature structure of early Mars

P. von Paris[a,b,*], F. Selsis[a,b], M. Godolt[c], J.L. Grenfell[c], H. Rauer[c,d], B. Stracke[c]

[a] *Univ. Bordeaux, LAB, UMR 5804, F-33270, Floirac, France*
[b] *CNRS, LAB, UMR 5804, F-33270, Floirac, France*
[c] *Institut für Planetenforschung, Deutsches Zentrum für Luft- und Raumfahrt (DLR), Rutherfordstr. 2, 12489 Berlin, Germany*
[d] *Zentrum für Astronomie und Astrophysik (ZAA), Technische Universität Berlin, Hardenbergstr. 36, 10623 Berlin, Germany*

Abstract

Ozone is an important radiative trace gas in the Earth's atmosphere and has also been detected on Venus and Mars. The presence of ozone can significantly influence the thermal structure of an atmosphere due to absorption of stellar UV radiation, and by this e.g. cloud formation. Photochemical studies suggest that ozone can form in carbon dioxide-rich atmospheres. Therefore, we investigate the effect of ozone on the temperature structure of simulated early Martian atmospheres.

With a 1D radiative-convective model, we calculate temperature-pressure profiles for a 1 bar carbon dioxide atmosphere containing various amounts of ozone. These ozone profiles are fixed, parameterized profiles. We vary the location of the ozone layer maximum and the concentration at this maximum. The maximum is placed at different pressure levels in the upper and middle atmosphere (1-10 mbar).

Results suggest that the impact of ozone on surface temperatures is relatively small. However, the planetary albedo significantly decreases at large ozone concentrations. Throughout the middle and upper atmospheres, temperatures increase upon introducing ozone due to strong UV absorption. This heating of the middle atmosphere strongly reduces the zone of carbon dioxide condensation, hence the potential formation of carbon dioxide clouds. For high ozone concentrations, the formation of carbon dioxide clouds is inhibited in the entire atmosphere. In addition, due to the heating of the middle atmosphere, the cold trap is located at increasingly higher pressures when increasing ozone. This leads to wetter stratospheres hence might increase water loss rates on early Mars. However, increased stratospheric H_2O would lead to more HO_x, which could efficiently destroy ozone by catalytic cycles, essentially self-limiting the increase of ozone. This result emphasizes the need for consistent climate-chemistry calculations to assess the feedback between temperature structure, water content and ozone chemistry. Furthermore, convection is inhibited at high ozone amounts, leading to a stably stratified atmosphere.

*Corresponding author: email vonparis@obs.u-bordeaux1.fr, tel. +33 (0)557 77 6131

Keywords:
early Mars: habitability, atmospheres

1. Introduction

The climate and, consequently, the habitability of early Mars are a long-standing question that has not yet been answered conclusively. From an atmospheric modeling point of view, short episodes of a warm, wet climate, followed by long periods of arid, cold climates, seem to be favored for the Noachian period about 3.8 billion years ago (e.g., Segura et al. 2008, Wordsworth et al. 2013, Halevy and Head 2014).

An important input for atmospheric modeling studies is the atmospheric composition, together with the surface pressure. Most previous studies (e.g., Kasting 1991, Wordsworth et al. 2013) assumed mixed carbon dioxide (CO_2)-water vapor (H_2O) atmospheres. In these studies, the partial pressure of carbon dioxide was of the order of bars, consistent with outgassing model studies (e.g., Phillips et al. 2001, Grott et al. 2011) and in-situ analyses (e.g., Manga et al. 2012, Kite et al. 2014). In 1D models, the atmospheric H_2O content is usually controlled by a fixed relative humidity to simulate a hydrological cycle.

However, other atmospheric (trace) gases such as molecular nitrogen (N_2), molecular hydrogen (H_2), methane (CH_4) or sulphur dioxide (SO_2) might have been present in the early Mars atmosphere. The initial N_2 inventory is thought to be relatively large (e.g., McKay and Stoker 1989) and can provide modest surface warming (von Paris et al. 2013b). Methane has also been suggested to warm the atmosphere (e.g., Postawko and Kuhn 1986, Ramirez et al. 2014), but the effect on surface temperature is small. Ramirez et al. (2014) find that H_2-induced warming could raise surface temperatures above freezing, assuming H_2 was a major atmospheric constituent (around 20 % volume mixing ratio). The effect of SO_2 has been investigated by a number of studies (e.g., Postawko and Kuhn 1986, Yung et al. 1997, Halevy et al. 2007, Johnson et al. 2008, Tian et al. 2010, Mischna et al. 2013), but results suggest that it most likely does not contribute strongly to warming the surface.

One proposed solution to warming early Mars has been the formation of carbon dioxide clouds (e.g., Pierrehumbert and Erlick 1998, Forget and Pierrehumbert 1997). Early 1D modeling studies suggested that the needed warming however strongly depends on the assumed cloud cover, which would have to be nearly 100% (e.g., Mischna et al. 2000). Following time-dependent 1D modeling studies by Colaprete and Toon (2003) found this to be unrealistic, a conclusion also supported by recent 3D studies (e.g., Forget et al. 2013, Wordsworth et al. 2013). In addition, Kitzmann et al. (2013) suggested that previous radiative transfer algorithms probably strongly overestimated the warming associated with carbon dioxide clouds.

The formation of carbon dioxide clouds depends on the temperature profile in the middle atmosphere. As shown by, e.g., Yung et al. (1997) or Ramirez et al. (2014), UV absorption by SO_2 or near-IR absorption by CH_4 can effectively inhibit carbon dioxide condensation, or at least reduce the cloud formation region.

So far, ozone (O_3) has not been considered in the context of early Mars. Like SO_2, ozone has strong UV and visible absorption bands. On Earth, these are responsi-

ble for the pronounced stratospheric temperature maximum. Ozone has been detected in the CO_2-rich atmospheres of both Venus (e.g., Montmessin et al. 2011) and Mars (e.g., Lebonnois et al. 2006). Furthermore, numerous photochemical modeling studies suggests that ozone can be formed from abiotically produced oxygen (e.g., Selsis et al. 2002, Segura et al. 2007, Domagal-Goldman and Meadows 2010; Domagal-Goldman et al. 2014). In addition, Wordsworth and Pierrehumbert (2014) propose a (non-chemical) abiotic oxygen formation process based on hydrogen escape and water cold-trapping. Therefore, it is reasonable to assume that on early Mars, ozone could have been also, to a certain extent, present in the atmosphere. Hence, in this study, we explore the effect of ozone on the temperature structure of early Mars

The paper is structured as follows: Section 2 presents the atmospheric model and the simulations performed. Results are shown and discussed in Sect. 3 and conclusions in Sect. 4.

2. Computational details

2.1. Model description

We use a 1D, steady-state, cloud-free radiative-convective atmosphere model to calculate globally, diurnally averaged temperature and H_2O profiles. The model is originally based on Kasting et al. (1984a) and Kasting et al. (1984b). Further code developments are described in, e.g., Kasting (1988), Mischna et al. (2000), von Paris et al. (2008) or von Paris et al. (2010).

The model atmospheres are divided into 52 levels. Temperature profiles in the upper atmosphere are obtained by solving the radiative transfer equation (38 bands for incoming stellar radiation, 25 bands for planetary and atmospheric thermal radiation). For incoming stellar radiation (0.2-4.5 μm), Rayleigh scattering (by N_2, H_2O, CO_2 and CH_4) and molecular absorption (by H_2O, CO_2, CH_4 and O_3) contribute to the opacity. To allow for scattering, the angular integration of the radiative transfer equation is performed using a 2-stream code (Toon et al. 1989). For thermal radiation (1-500 μm), molecular absorption (by H_2O, CO_2, CH_4 and O_3, see below, Sect. 2.2) and continuum absorption (by N_2, H_2O and CO_2) are considered. N_2 continuum data is taken from Borysow and Frommhold (1986) and Lafferty et al. (1996), whereas H_2O self and foreign continua as well as the CO_2 foreign continuum are incorporated following Clough et al. (1989). The CO_2 collision-induced self continuum is described following Kasting et al. (1984b). In the lower atmosphere, the model performs convective adjustment such that temperature profiles follow the wet adiabat. The formulation of the adiabatic lapse rate takes into account the condensation of H_2O or CO_2 (Kasting 1991). The super-saturation ratio for the onset of CO_2 condensation is unity (but see Glandorf et al. (2002) for a different estimate for early Mars).

H_2O profiles are re-calculated for each model time step, according to local temperature and using a fixed relative humidity (RH) profile. The concentrations of the other species are fixed at the start of the calculations and only adjusted according to condensation of water and carbon dioxide at the surface (von Paris et al. 2013a).

For more details, we refer to von Paris et al. (2008) and references therein.

Table 1: Spectral intervals for the new IR radiative transfer scheme and species considered

Interval	range [cm^{-1}]	contributing species
1	7,470 - 10,000	CO_2,H_2O,CH_4
2	6,970 - 7,470	CO_2,H_2O,CH_4
3	6,000 - 6,970	CO_2,H_2O,CH_4
4	5,350 - 6,000	CO_2,H_2O,CH_4
5	4,600 - 5,350	CO_2,H_2O,CH_4
6	4,100 - 4,600	CO_2,H_2O,CH_4
7	3,750 - 4,100	CO_2,H_2O,CH_4
8	3,390 - 3,750	CO_2,H_2O,CH_4
9	3,050 - 3,390	CO_2,H_2O,CH_4
10	2,750 - 3,050	CO_2,H_2O,CH_4
11	2,400 - 2,750	CO_2,H_2O,CH_4
12	2,250 - 2,400	CO_2,H_2O,CH_4
13	2,150 - 2,250	CO_2,H_2O,CH_4,O_3
14	2,000 - 2,150	CO_2,H_2O,CH_4,O_3
15	1,850 - 2,000	CO_2,H_2O,CH_4,O_3
16	1,400 - 1,850	CO_2,H_2O,CH_4,O_3
17	1,100 - 1,400	CO_2,H_2O,CH_4,O_3
18	1,000 - 1,100	CO_2,H_2O,CH_4,O_3
19	905 - 1,000	CO_2,H_2O,CH_4,O_3
20	820 - 905	CO_2,H_2O,CH_4,O_3
21	730 - 820	CO_2,H_2O,O_3
22	600 - 730	CO_2,H_2O,O_3
23	525 - 600	CO_2,H_2O,CH_4,O_3
24	460 - 525	CO_2,H_2O,CH_4
25	20 - 460	H_2O,CH_4,O_3

2.2. Model improvements

The original IR radiative transfer scheme MRAC (as used in, e.g., von Paris et al. 2008, von Paris et al. 2010, von Paris et al. 2013b) only considered gaseous absorption by H_2O and CO_2 for the calculation of opacities. For this work, a new, updated MRAC version has been created that also considers CH_4 and O_3 for gaseous absorption.

Table 1 shows the spectral intervals as well as the species included in these intervals.

Line positions and line strengths for both CH_4 and O_3 have been taken from the Hitran 2008 database (Rothman et al. 2009). Line strengths are converted from the reference temperature of 296 K to the desired temperature following Norton and Rinsland (1991). Cross sections are then obtained with the MIRART-Squirrl line-by-line radiative transfer code (Schreier and Schimpf 2001; Schreier and Böttger 2003) using 10^6 spectral points per band. The line shape is taken to be a Voigt line profile with a cutoff of $10\,cm^{-1}$. The foreign component of the Lorentz broadening is taken directly from the Hitran database, i.e. for air. The self component of the Lorentz broadening was calculated assuming a volume mixing ratio (vmr) of 10^{-6} for both CH_4 and O_3,

Table 2: Interpolation and range of the grid variables in the new IR radiative transfer scheme

Quantity	Range	Interpolation	Comments
Temperature	100-400 K	linear in T	Δ T=50 K
Pressure	10^{-5}-1.5 bar	linear in log(p)	Δ log(p)=0.1
H_2O concentration	10^{-9}-1	linear in vmr	1-4 points per order of magnitude
carbon dioxide concentration	10^{-6}-1	linear in vmr	1-4 points per order of magnitude
CH_4 concentration	10^{-8}-10^{-2}	linear in vmr	1-4 points per order of magnitude
O_3 concentration	10^{-8}-10^{-2}	linear in vmr	1-4 points per order of magnitude

$3.55{\cdot}10^{-4}$ for CO_2 and 10^{-3} for water. Numerical tests showed that except for high water concentrations ($\gtrsim 10^{-2}$), the effect of the self component on the cross sections was negligible.

The chosen line cutoff in this work is relatively short. Tests with a line-by-line radiative transfer code with line cut-offs at 25 cm^{-1} have shown that the overall flux change rarely exceeds 5 % in a given spectral band. For the total integrated outgoing thermal flux, we find a difference of about 1 %, equal to a radiative forcing of a few W m^{-2}. This could lead to a small change in surface temperature of a few K (see also, for example, Wordsworth et al. 2010). However, this is not expected to qualitatively alter our conclusions. Furthermore, as pointed out by, e.g., Halevy et al. (2009), Wordsworth et al. (2010) or Mischna et al. (2012), assuming a Voigt line profile is probably not a well-justified choice in dense CO_2 atmospheres where the far wings of lines are substantially sub-Lorentzian. Sensitivity tests by Wordsworth et al. (2010) or von Paris et al. (2010) showed that the influence on surface temperature can be large (of the order of 10 K). Still, this is again not likely to influence the conclusions regarding the impact of ozone on the thermal structure in the upper and mid atmosphere.

The interpolation variables are temperature, log(pressure) and the individual concentrations c_i of the absorbing species. The concentration grid has four dimensions, one for H_2O, CO_2, CH_4 and O_3, respectively. Table 2 summarizes the range of the interpolation variables and the type of interpolation.

Figure 1 illustrates our approach to calculate the needed k distributions. In every spectral interval, for each temperature-pressure point (T/p), cross sections σ_i have been calculated for the contributing species i (see Table 1). These are then combined to obtain effective cross sections σ_{eff} for the different gas mixtures according to assumed molecular concentrations c_i from Table 2:

$$\sigma_{\mathrm{eff}} = \sum_i c_i \cdot \sigma_i \tag{1}$$

From the effective cross sections σ_{eff}, k distributions have been obtained that are then used in the model for the radiative transfer calculations with a correlated-k approach.

2.3. Model verification

We tested the new model against results for early Mars from von Paris et al. (2013b). As an example, Figure 2 shows the temperature profiles and differences for a 1 bar car-

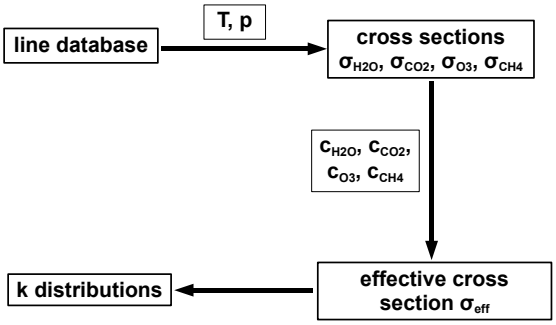

Figure 1: Flowchart for calculation of k distributions.

bon dioxide case (without N_2). It is clearly seen that both models compare relatively well with each other. The small discrepancies are due to a slightly different approach to calculate the line broadening parameters for the k distributions at high pressures, compared to earlier work (e.g., von Paris et al. 2008, 2010). In the line-by-line radiative transfer code used to calculate the cross sections (see above), the broadening pressure p_b of the gas species i is calculated from the ideal gas law, i.e. $p_b = c_i \cdot p$ instead of using a column-density correction to calculate the actual broadening pressure (e.g., see Kasting 1987). However, these differences do not affect the conclusions of previous studies.

The second model verification uses a modern Earth reference profile. Ozone and methane concentrations were taken from Grenfell et al. (2011). We run simulations with two different thermal radiative transfer schemes. First, we used RRTM (Mlawer et al. 1997), a scheme that is widely used in 1D and 3D exoplanet and Earth climate studies (e.g., Segura et al. 2003, 2005, Roeckner et al. 2006, Grenfell et al. 2007b, Kaltenegger et al. 2011, Stevens et al. 2013). A second simulation was done with the new scheme presented in this work.

Figure 3 shows the resulting temperature profiles (left panel), the temperature difference between both models (center panel) and a flux comparison for the upwelling thermal flux (right panel). For the latter, we compared calculated model IR fluxes with fluxes calculated by the high-resolution line-by-line code MIRART-Squirrl.

Concerning the temperature profiles, the agreement in the troposphere and the lower stratosphere is very good. In the upper stratosphere, small discrepancies can be seen, reaching up to about 3 K. However, the overall agreement is good, and such small temperature differences are not expected to have a large influence neither on observables (e.g. spectral signatures) nor on temperature-dependent chemistry. For the IR thermal upwelling flux, it is clearly seen that the fluxes do not differ by more than a few % throughout the stratosphere.

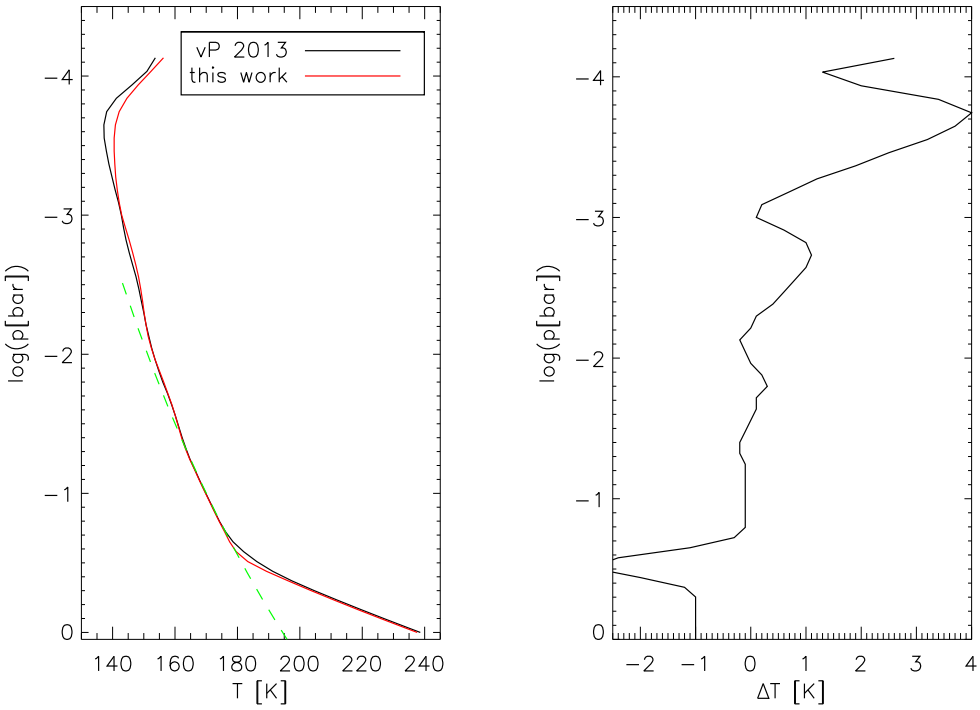

Figure 2: Early Mars: Comparison of temperature profiles from von Paris et al. (2013b) and this work. Carbon dioxide saturation vapor pressure curve as green dashed line.

Based on these verifications, we consider the new radiative scheme to be applicable to further planetary scenarios.

2.4. Early Mars scenarios

Simulated model atmospheres were assumed to be composed of CO_2, H_2O and O_3. The CO_2 partial pressure is fixed at 1 bar, consistent with upper limits placed on atmospheric pressure during the Noachian (e.g., Phillips et al. 2001). H_2O is calculated according to ambient temperature, assuming a fully saturated atmosphere (i.e., RH=1, see von Paris et al. 2013b). This approach is similar to most 1D studies of early Mars (e.g., Mischna et al. 2000, Colaprete and Toon 2003, Tian et al. 2010), but most likely over-estimates the amount of atmospheric water. The surface albedo was set to 0.21, close to the observed value of present Mars (Kieffer et al. 1977). This value of surface albedo allows the model to reproduce present Mars mean surface temperatures. Planetary gravity is 3.73 ms^{-2}, and the orbital distance is set to 1.52 AU. We neglected any effect of eccentricity. However, even though Mars' orbit is eccentric today (e=0.09), and eccentricity cycles would occasionally drive the eccentricity to high values (e.g.,

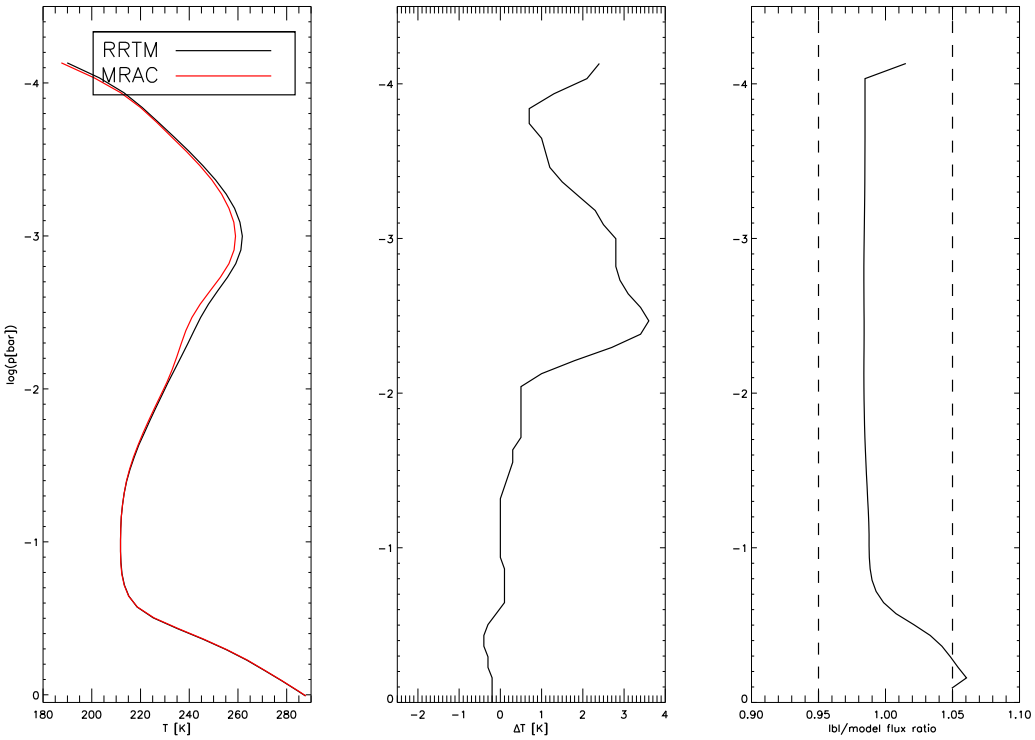

Figure 3: Modern Earth model verification: (Left panel) Comparison of temperature profiles calculated with RRTM (Mlawer et al. 1997) and MRAC (this work). (Center panel) ΔT (RRTM-MRAC) between both models, (Right panel) IR upwards flux ratio (climate model)/line-by-line.

Laskar et al. 2004), the overall effect would probably be small (at e=0.2, the mean flux increases by only 2 % compared to the circular case).

The incoming solar irradiation was set to Noachian conditions 3.8 billion years ago, i.e. 75 % of today's irradiation (e.g., Gough 1981). The input spectrum was taken from Gueymard (2004) and scaled at all wavelengths accordingly. Note that this approach is consistent with previous early Mars studies (e.g., Kasting 1991, Tian et al. 2010, Wordsworth et al. 2013). Other work, primarily on early Earth climate, not only scaled the spectrum, but also incorporate the variation of stellar parameters (e.g., Goldblatt et al. 2009) and enhanced UV radiation (e.g., Kunze et al. 2014). Enhanced UV radiation (see, e.g., Ribas et al. 2005) of the young Sun could have played an especially important role affecting ozone hence the thermal structure of the atmosphere.

Ozone profiles strongly depend on the assumed oxygen content of the atmosphere, the incoming stellar UV radiation, and, in addition, on the catalytic cycles (HO_x, NO_x, etc.) operating in the atmosphere (e.g., Selsis et al. 2002, Segura et al. 2007, Grenfell et al. 2013). Detailed photochemical modeling is warranted for this problem, however such relatively complex models would necessitate many more unconstrained bound-

ary conditions and parameters (such as surface fluxes of oxidizing and reducing compounds, wet and dry deposition rates, vertical mixing, kinetic data, UV radiation field, etc.). Such complex models (e.g., Selsis et al. 2002, Segura et al. 2007, Hu et al. 2012, Domagal-Goldman et al. 2014, Tian et al. 2014, Grenfell et al. 2014) allow for an estimate of possible ranges of ozone concentrations. Motivated by the results from detailed photochemical studies, we perform a sensitivity study of the influence of ozone on temperature structure by inserting artificial ozone profiles C_{O_3}. These profiles are not the output of a photochemical model, but are parameterized as a function of pressure p based on a Gaussian profile

$$C_{O_3}(p) = \mathrm{vmr}_{\mathrm{max}} \cdot \exp\left(-\frac{\left(\log\frac{\mathrm{p}}{\mathrm{p}_{\mathrm{max}}}\right)^2}{0.5}\right) \tag{2}$$

where p_{max} is the pressure of the maximum concentration and $\mathrm{vmr}_{\mathrm{max}}$ is the maximum volume mixing ratio.

We performed simulations for different combinations of $\mathrm{vmr}_{\mathrm{max}}$ and p_{max}, as shown in Table 3. In Fig. 4, we show a sample of the chosen ozone profiles, together with a modern Earth mean profile.

Table 3: Adopted parameter values for eq. 2 in this work.

Parameter	Values
p_{max} [mbar]	0.1, 1, 10
$\mathrm{vmr}_{\mathrm{max}}$ [ppm]	0.1, 1, 10, 100

The ozone layer peak (its location and its magnitude) is the result of an interplay between two main effects. On the one hand, ozone formation requires photolytic release ($\lambda \lesssim 200$ nm) of atomic oxygen (O) e.g. from O_2, CO_2, H_2O, which are usually more abundant on the lower levels (followed by fast, three-body formation of ozone). On the other hand, UV radiation is more abundant with increasing altitude, hence there is generally a distinct maximum of ozone concentration at pressures of about 10^{-4}-10^{-2} bar. This motivates the form of our artificial ozone profiles.

Previous calculations by, e.g., Selsis et al. (2002) and Segura et al. (2007) suggest a maximum in ozone number density of up to 10^{12} cm^{-3}, located at pressures around 1-10 mbar. They found ozone columns between 10^{-4}-2 times the modern Earth column (Table 3 in Selsis et al. 2002 and Table 2 in Segura et al. 2007). Both studies focused on N_2- or CO_2-rich atmospheres, similar to the ones considered here. The oxygen needed for ozone formation was either provided by H_2O or CO_2. To cover the entire range of possible ozone concentrations found by Selsis et al. (2002) (i.e., their humid and dry CO_2 cases as possible extremes) we varied the maximum ozone concentration between 0.1 and 100 ppm. As shown in Table 4, this leads to relatively thick ozone columns (up to 24x the modern Earth values) for a few cases.

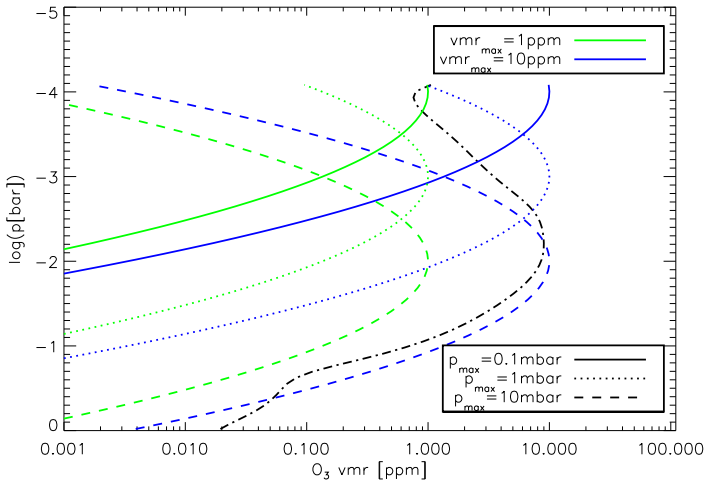

Figure 4: Sample of chosen ozone profiles. Earth mean profile from Grenfell et al. (2011) as dash-dotted line.

Table 4: O_3 columns (in units of terrestrial columns, where one terrestrial column corresponds to 315 Dobson units) for the scenarios listed in Table 3.

p_{max} [mbar] \ vmr_{max} [ppm]	0.1	1	10	100
0.1	0.00023	0.0023	0.023	0.23
1	0.00249	0.0249	0.249	2.48
10	0.0248	0.248	2.47	24.7

3. Results and Discussion

3.1. Surface temperature

Figure 5 shows the surface temperature as a function of the parameters in eq. 2.

For all scenarios, the surface temperatures first slightly increase with increasing vmr_{max}, due to a slight decrease of planetary albedo and an additional greenhouse effect from ozone. For higher vmr_{max}, surface temperatures start to decrease with vmr_{max} (see below).

However, for the p_{max}=0.1 and 1 mbar cases, the overall effect is rather small, of the order of 1-2 K. In contrast, for p_{max}=10 mbar, the increase at low vmr_{max} (up to 2 K) and the subsequent decrease towards higher values is much more pronounced, with a maximum temperature drop of about 8 K compared to the zero-ozone case.

3.2. Temperature structure

Figure 6 shows the effect of ozone on the calculated temperature-pressure profiles. In the middle and upper atmosphere, up to 60 K of warming is seen, depending on

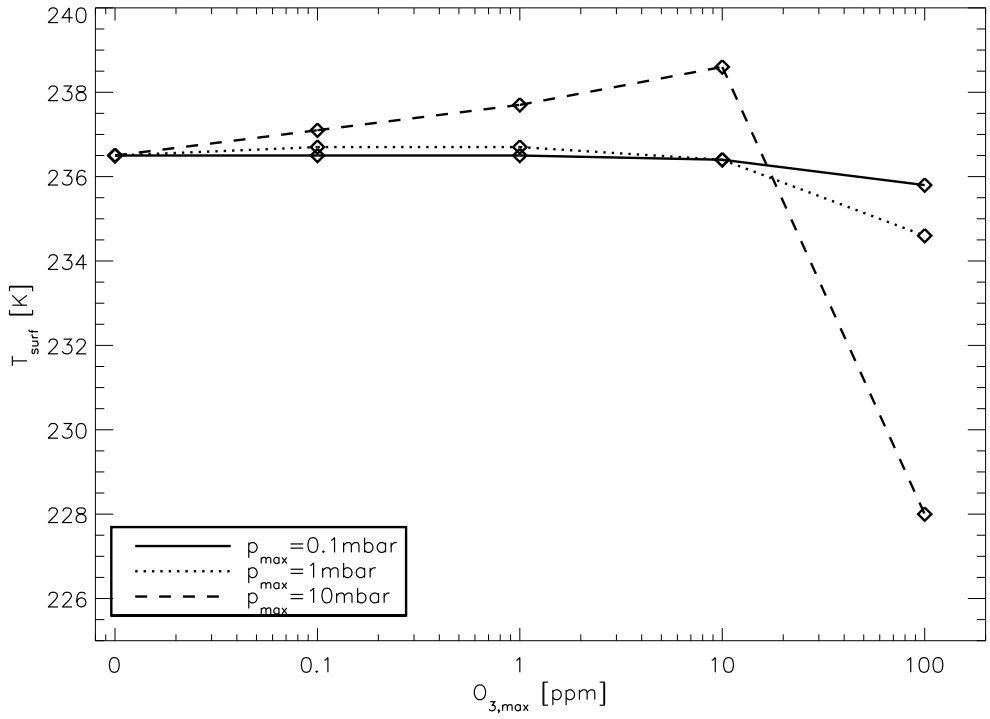

Figure 5: Effect of ozone on surface temperature.

the choice of O_3 parameters. This is of course due to the massive increase in stellar heating rates associated with the absorption of solar UV absorption by ozone. Heating rates increase by up to a factor of 5 compared to the no-ozone case (not shown).

Two other effects are readily inferred from Fig. 6. First, for the $p_{\rm max}$=10 mbar cases at $\rm vmr_{max}$=10 and 100 ppm, temperature profiles no longer follow the carbon dioxide saturation pressure curve (black dashed line in Fig. 6). This suggests that carbon dioxide condensation, hence also the formation of carbon dioxide clouds, is prohibited throughout the entire atmosphere. For the other cases, the potential cloud formation zone is reduced, although the effect is rather minimal at low $\rm vmr_{max}$ or small $p_{\rm max}$. Second, as suggested by the slope of the $\rm vmr_{max}$=100 ppm, $p_{\rm max}$=10 mbar case, the lower atmosphere is no longer convective. This is in contrast to the other scenarios, where the lapse rate follows a CO_2 adiabat in the mid atmosphere and a wet H_2O adiabat in the lower atmosphere.

The strong UV absorption by ozone drastically changes the energy balance in the atmosphere. Figure 7 illustrates the effect of ozone on the planetary albedo. The planetary albedo is reduced by up to 40 % at large ozone layers. In terms of additional radiative energy deposited into the atmosphere, a reduction of albedo from 0.32 (zero-ozone) to 0.2 (maximum ozone effect) corresponds to a forcing of 13 $\rm Wm^{-2}$. However,

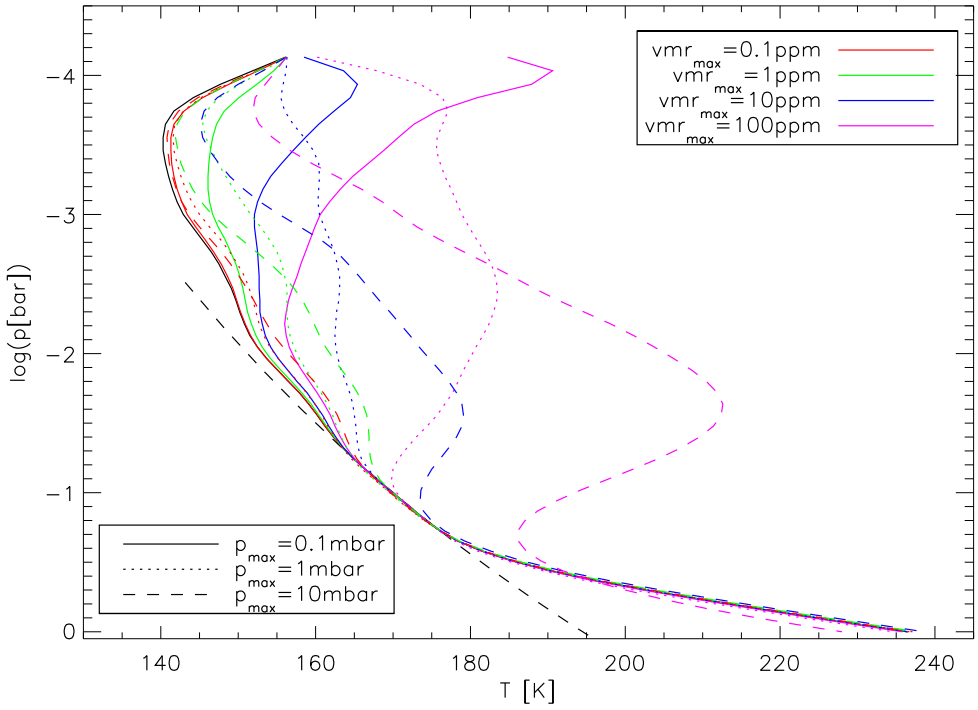

Figure 6: Effect of ozone on temperature structure. Reference case (zero ozone) as black plain line. Carbon dioxide saturation pressure shown as black dashed line.

as illustrated in the left panel of Fig. 8, most of this energy is absorbed in the middle atmosphere. As a consequence of the strong absorption, the incoming solar flux at the surface is reduced by about 20 %. Therefore, the total radiative flux in the lower atmosphere (sum of stellar and thermal fluxes) is reduced, coming closer to radiative equilibrium. Hence, less energy is available to drive convection. This then leads to a radiative instead of a convective lower atmosphere (as observed in Fig. 6).

A reduced albedo corresponds to a larger thermal flux that must be emitted by the atmosphere to satisfy energy balance and radiative equilibrium at the top of the atmosphere. For optically thin atmospheres such as Earth's, this generally leads to an increase in surface temperature. In the case of dense carbon dioxide-dominated atmospheres considered here, the thermal emission originates mostly from pressures at around 10-100 mbar, since at higher pressures, the atmosphere is optically thick for thermal radiation at all wavelengths (see right panel of Fig. 8). For the considered scenarios with a substantial increase of local temperature (see Fig. 6), the local IR flux also increases. This balances the solar flux deposited in the atmosphere. Most of the outgoing thermal flux stems from emission in the 15 μm band of carbon dioxide which becomes optically thick at pressures around 10-100 mbar.

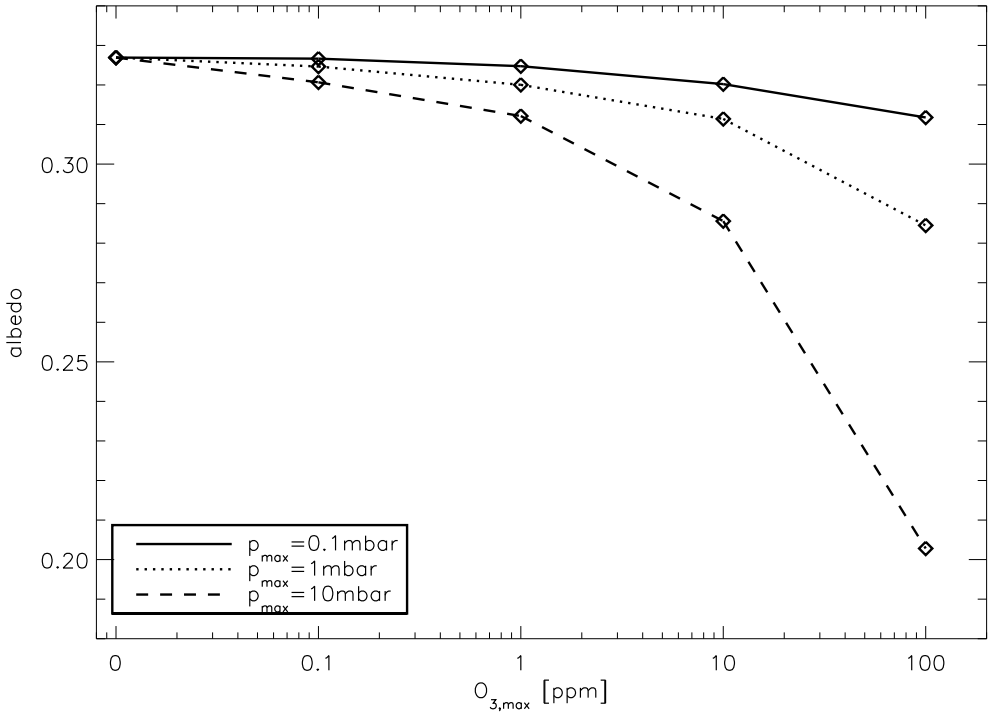

Figure 7: Effect of ozone on calculated planetary albedo.

3.3. Discussion

3.3.1. Oxygen content and catalytic chemistry

The assumed ozone profiles are dependent on the oxygen content of the early Mars atmosphere. Given that modern Mars has only little oxygen in the atmosphere (around 10^{-3} vmr, e.g., Yung and deMore 1999), it seems likely that our high-ozone cases will over-estimate the total ozone column by a generous margin. However, the formation of ozone also depends on the assumed UV radiation field (e.g., Segura et al. 2007, Domagal-Goldman and Meadows 2010, Domagal-Goldman et al. 2014, Grenfell et al. 2014, Tian et al. 2014) which is relatively poorly known for the young Sun (Ribas et al. 2005). Observations of younger solar-type stars suggest that far-UV and X-ray emissions strongly decrease with age (e.g., Ribas et al. 2005) whereas the total luminosity is generally assumed to increase with age (e.g., Gough 1981, Caldeira and Kasting 1992). Therefore, the ratio between oxygen (hence ozone) production via photolysis (in the far-UV) and photolytic ozone destruction (in the near-UV) could presumably change dramatically and produce largely varying ozone concentrations (see, e.g., sensitivity studies by Segura et al. 2007, Grenfell et al. 2014 or Tian et al. 2014). Therefore, reliable quantitative estimates of ozone on early Mars are challenging to obtain. Detailed photochemical models would probably only allow for an order-of-magnitude estimate

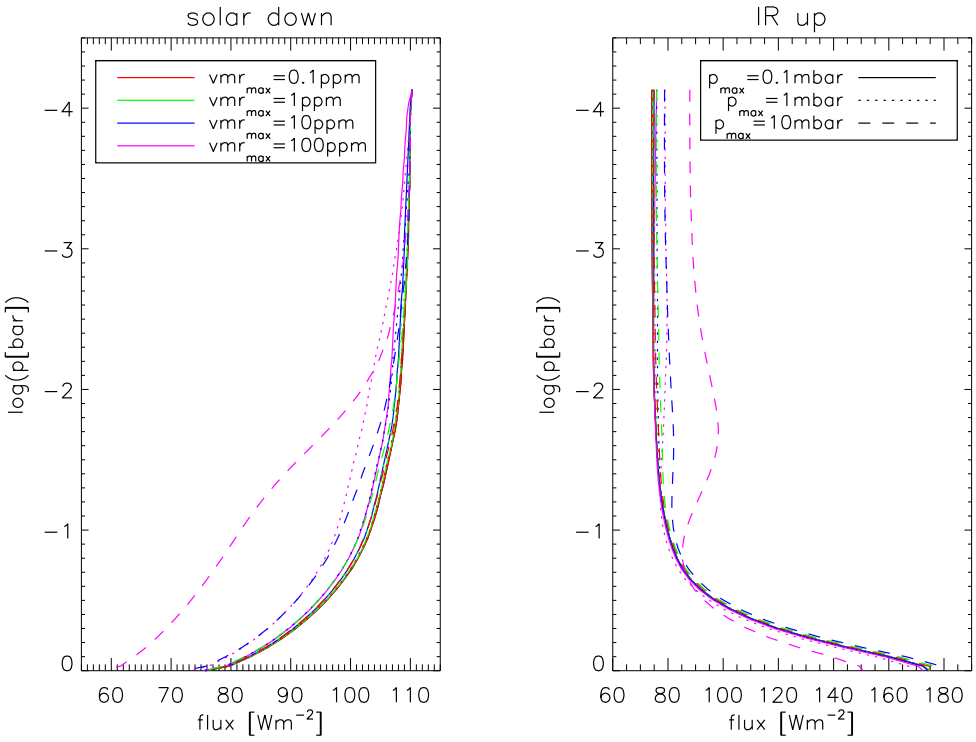

Figure 8: Effect of ozone on downwards solar (left) and upwelling thermal fluxes (right). Captions correspond to both panels.

of such quantities, since boundary conditions (such as wet deposition of hydrogenated species and oxidation of reduced volcanic gases) are essentially unconstrained.

In addition, ozone chemistry heavily depends on the operating catalytic cycles in the atmosphere (e.g., Crutzen 1970, Grenfell et al. 2013). On Earth, most of the cycles are related to NO_x and HO_x. Possible NO_x sources on early Mars would be cosmic rays (e.g., Jackman et al. 1980) or lightning (e.g., Segura and Navarro-González 2005), but these are hard to estimate. It is unclear whether significant HO_x cycles could operate on early Mars, since calculated stratospheres are very dry (see Fig. 9), with vmr about 10^{-8}-10^{-6}. This is up to several hundred times drier than in the modern Earth stratosphere (H_2O vmr of a few times 10^{-6} up to 10^{-5}). Note, however, that HO_x cycles are responsible for the low oxygen content in the present Mars atmosphere (e.g., Nair et al. 1994, Yung and deMore 1999, Stock et al. 2012a,b) since they quickly recycle the products of CO_2 photolysis (CO+O) back to CO_2. Without such recycling, the martian atmosphere would be more O_2-rich than today, probably at around 5-10 % O_2. CO_2 would still remain the dominant atmospheric species (e.g., Nair et al. 1994). This can be explained by the fact that at increasingly higher O_2 concentrations, O_2 UV absorption starts to shield the CO_2 from becoming photolyzed since O_2 photodissociation

cross sections are much larger than corresponding CO_2 cross sections (see, e.g., Yung and deMore 1999, Selsis et al. 2002). Even on Venus with a very dry stratosphere, HO_x cycles operate, using HCl photolysis as source for H (Yung and deMore 1999). As an alternative destruction cycle, SO_x cycles could be possible, since higher amounts of sulphur-bearing species are expected in the early Mars atmosphere (e.g., Farquhar et al. 2000, Halevy et al. 2007, Johnson et al. 2008, Ramirez et al. 2014).

Investigating these possibilities is however beyond the scope of this sensitivity study that focuses on climatic effects.

3.3.2. Eddy diffusion and convection

As a result of the suppression of convection in the lower atmosphere (see Fig. 6) for the high-ozone case, the atmosphere becomes stably stratified and vertical transport is significantly reduced. This has a potentially large impact on (photo)chemistry in such atmospheres. In general, photochemical networks include photochemical reactions (including e.g. 3-body reactions, photolysis, decomposition reactions, etc.) as well as a vertical mixing, which is parameterized by so-called Eddy diffusion. For the convective troposphere, 1D photochemical models of Mars or Earth use constant, relatively high, Eddy diffusion coefficients (e.g., Massie and Hunten 1981, Yung and deMore 1999). In a stably stratified atmosphere, the diffusion is most likely less efficient. The magnitude of the effect on convection and transport depends, among others, on the topography. Thus, full 3D dynamic simulations are probably needed to investigate the influence on chemistry. This is, for modern Earth and Earth-like **(terrestrial)** exoplanets, mostly important for biogenic trace gases such as methane and nitrous oxide. In the lower atmosphere, these are more strongly influenced by transport rather than chemistry (e.g., Segura et al. 2003, 2005 Grenfell et al. 2007a,b).

Exploring this issue, while beyond the scope of this work, would however be interesting in the context of fully coupled climate-chemistry simulations.

3.3.3. Water loss from early Mars

The very thin atmosphere of current Mars is likely shaped by significant atmospheric loss. Isotopic signatures of atmospheric escape have been found for nitrogen and oxygen (e.g., Jakosky and Phillips 2001, Fox and Hać 2010, Gillmann et al. 2011). Recent D/H isotopic ratio measurements of the Curiosity rover on Mars suggest that hydrogen escape and water loss has been ongoing over the last few billion years (e.g., Mahaffy et al. 2015) after the (presumed to be dense) Noachian atmosphere has been eroded. Modeling the escape of water is a very important issue for atmospheric evolution and habitability (e.g., Kasting 1988, Kulikov et al. 2006). The water loss rate depends on the stratospheric water content, where water is photolyzed and subsequent loss of H atoms occurs (e.g., Kasting 1988, Kasting et al. 1993).

Figure 9 shows the calculated H_2O profiles. Note that we assume a relative humidity of unity throughout the atmosphere hence H_2O concentrations are likely to be over-estimated in the mid- to upper atmosphere. On Earth, the stratospheric H_2O content is mainly controlled by the efficient cold trap near the tropopause (around 10 km altitude). With increasing temperatures due to the ozone layer, water is efficiently trapped in the troposphere. This leads to the dry stratosphere and, consequently, low water escape rates.

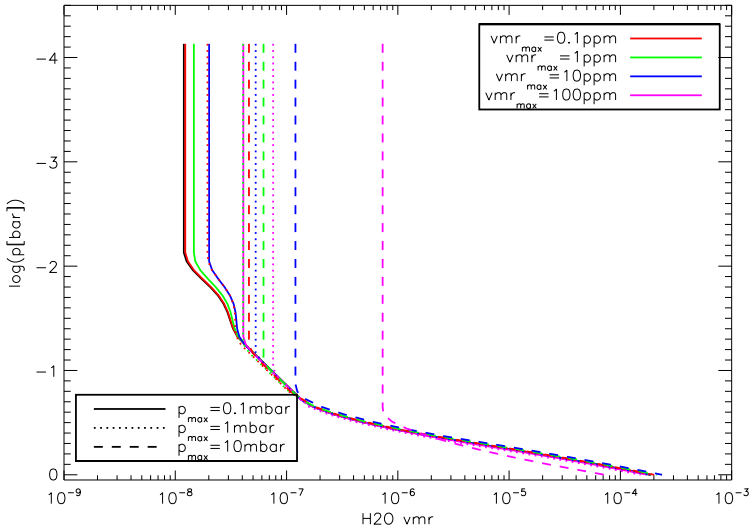

Figure 9: Effect of ozone on calculated water profiles.

For the early Mars scenarios considered here, cold traps develop even in the absence of temperature inversions. However, given that surface temperatures are very low, and the cold trap is located high in the atmosphere, stratospheric H_2O concentrations are very low. This suggests that water loss might be very slow on early Mars. However, when increasing the ozone concentrations in the model atmospheres, the altitude of the cold trap changes dramatically, due to the change in the temperature structure (see Fig. 6). This leads to a significant increase of stratospheric H_2O content (up to two orders of magnitude), and possibly impacts the water escape rates. Hence, results suggest that water escape rates might be sensitively influenced by the ozone content. Note, however, that an increase in stratospheric H_2O concentrations could also lead to enhanced destruction of ozone through catalytic HO_x chemistry (see, e.g., the parametric simulations of Tian et al. 2014). Therefore, changes in cold-trap locations might limit the increase of ozone, hence limit also H_2O escape. To further investigate this issue would need consistent climate-chemistry models to assess this feedback between vertical temperature structure, stratospheric water content and ozone chemistry.

To estimate the amount of water lost via atmospheric escape, we adopted the same approach as Wordsworth and Pierrehumbert (2014). Escape was assumed to be diffusion-limited and controlled by the cold-trap temperature T_{ct} and cold-trap water concentrations. The diffusion coefficient of H_2O through a CO_2 atmosphere was taken from approximative equations of Marrero and Mason (1972).

These approximations lead to water escape fluxes of, even under the most favorable escape conditions, only about 1 cm of water lost within 10^9 years (1 Gyr). This has to be compared to the actual atmospheric water column of about a few 10^{-4} m of water in our simulations. Furthermore, the original Martian water inventory is estimated to be much

larger, about 10^2-10^3 m (e.g., McKay and Stoker 1989, Lammer et al. 2013, Lasue et al. 2013), Currently, most of the water is thought to either reside in the cryosphere or to be bound to minerals in the crust (see discussion in, e.g., Lammer et al. 2013 and Lasue et al. 2013).

In addition, we point out that current best estimates of the hydrogen escape flux suggest about 1-2 m of water lost in 1 Gyr (e.g., Chassefière and Leblanc 2004, Zahnle 2015), about 2 orders of magnitude more than we calculate. This is due to the fact that molecular and atomic hydrogen are the main hydrogen-bearing species in the upper Martian atmosphere, not H_2O, as we assumed above. H and H_2 have concentrations about 2 orders of magnitude higher than H_2O (e.g., Nair et al. 1994, Yung and deMore 1999). H and H_2 are derived from H_2O photolysis, and since water is controlled by surface conditions and constantly replenished, H and H_2 can build up until concentrations reach an equilibrium between the photolytic source and atmospheric escape. Addressing the connection between cold-trap location, thermal structure and H_2O escape necessitates coupled climate-chemistry simulations, which is a potential direction of future research.

3.3.4. Spectral appearance

In an exoplanetary context, an interesting question with respect to ozone is the possibility of detecting it remotely with spectroscopic observations. It has been proposed as a so-called biosignature gas (e.g., Léger et al. 1996, Selsis 2000, Schindler and Kasting 2000, Des Marais et al. 2002, Selsis et al. 2002), and much work has been invested into atmospheric and spectral modeling regarding detection and interpretation of ozone signatures (e.g., Selsis et al. 2002, Segura et al. 2003, 2007, Kaltenegger et al. 2007, Kaltenegger and Traub 2009, Rauer et al. 2011, Hedelt et al. 2013, Grenfell et al. 2014).

Considering early Mars as a potential exoplanet, Fig. 10 shows the resulting emission spectra for five selected cases. They have been calculated with the same high-resolution line-by-line code used for the model verification (Schreier and Böttger 2003) and were then binned to a coarse spectral resolution of R=$\frac{\lambda}{\Delta\lambda}$=100. As pointed out by Selsis et al. (2002), the ozone band at 9.6 μm coincides with a carbon dioxide hot band and lies in the wings of the strong dimer absorption feature (see, e.g., Wordsworth et al. 2010 for the most recent carbon dioxide continuum absorption data). Therefore, except for the strongest ozone column, the shape of the spectral band is not greatly sensitive to atmospheric ozone amount.

To illustrate this, Fig. 11 zooms in on the spectral region around the 9.6 μm fundamental band of ozone. For comparison, we also show line-by-line calculations with removed ozone (marked "no O3" in Fig. 11) to investigate the effect of ozone on the spectral appearance and a possible masking by CO_2. It is clear that an effect is only seen for the highest ozone columns (higher than the modern-day terrestrial column, Table 4). To detect this, relatively high spectral resolution (here, R=100) and reasonable signal-to-noise ratios (of the order of 4) are needed. These values are not achievable with currently planned instrumentation even for Earth-sized or larger planets, let alone a planet the size of Mars (see, e.g., Hedelt et al. 2013).

The strong carbon dioxide fundamental band around 15 μm is very sensitive to middle-atmosphere temperatures (see Fig. 8), and the effect of the changing temper-

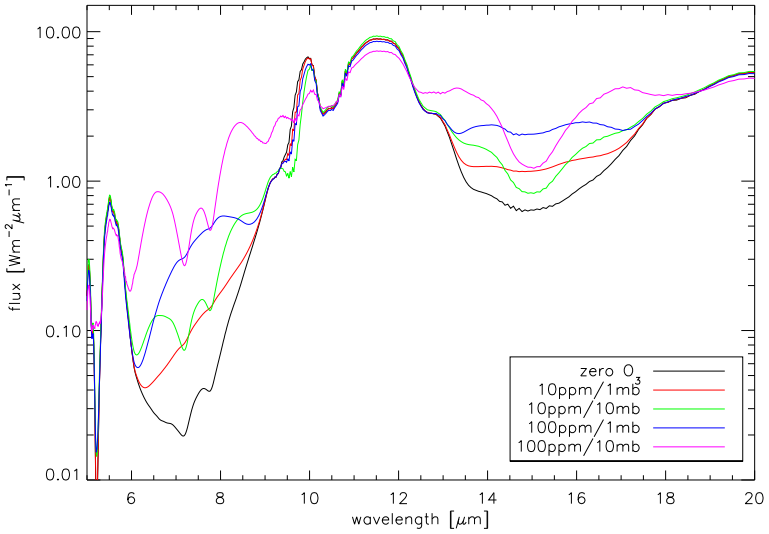

Figure 10: Emission spectra (spectral resolution R=100) for selected cases.

ature structure is clearly apparent in this band. In the hypothetical case that all stellar parameters (including UV radiation field) were known, and consistent atmospheric modeling were used, then this band would constitute an excellent indirect probe of atmospheric ozone content. We note, however, that other radiative gases could also be responsible for a temperature inversion (e.g., SO_2, CH_4, etc.). This then is an important challenge for retrieval algorithms (e.g., von Paris et al. 2013c, Irwin et al. 2014).

In addition to that, the broad 6.3 μm band of water, superimposed by part of a carbon dioxide dimer absorption feature, is also sensitive to middle-atmosphere temperatures and thus would be an indirect probe of ozone content.

Summarizing, in the cases considered for this work, ozone is hardly seen directly in the spectra, except at high ozone contents. Indirectly, however, due to its impact on the thermal structure, the effect of ozone is clearly seen in the spectra.

As outlined in Kitzmann et al. (2011) or von Paris et al. (2013d), we use the model output of the stellar radiative transfer code to produce low-resolution albedo spectra. In Fig. 12, we show the UV-visible part of the spectrum. For the low-ozone reference case, the spectral albedo clearly follows the Rayleigh scattering slope expected for dense carbon dioxide atmospheres. The presence of ozone leads to a strong reduction of albedo in the Hartley (0.24 μm< λ<0.34 μm) and Chappuis (0.4 μm< λ <0.7 μm) bands. Additionally, the location of the ozone maximum also influences the spectral albedo in the Hartley band, as shown in Fig. 12. For cases where the maximum is located at higher pressures, the UV radiation penetrates deeper into the atmosphere and thus is more susceptible to Rayleigh scattering by carbon dioxide.

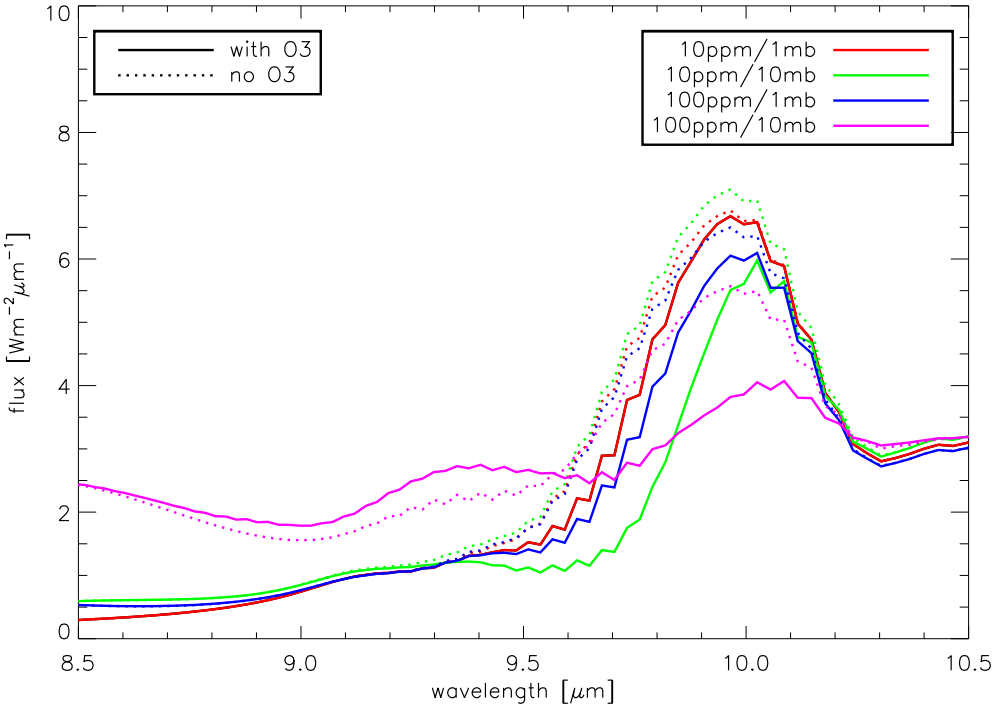

Figure 11: Zoom in the 9.6 μm band of ozone. Effect of including ozone in spectral calculations (R=100).

4. Conclusions

Ozone is a radiatively important atmospheric species due to strong UV absorption bands. It can significantly change the atmospheric temperature structure and thus affect, e.g., cloud formation or atmospheric transport.

We have investigated the influence of ozone on the atmospheric temperature structure of early Mars. We simulated a 1 bar carbon dioxide atmosphere with different, fixed ozone concentration profiles. To do this, we have developed a new IR radiative transfer scheme that incorporates molecular absorption of carbon dioxide, water, methane and ozone. Calculated IR cross sections cover a wide range of temperatures, pressures and concentrations. Hence, this scheme can be applied to a wide range of possible planetary scenarios.

Results suggest that the impact on surface temperatures at small to moderate ozone concentrations is probably not large, of the order of 1-3 K, depending on the overall ozone column. The increase in surface temperature is mostly due to the decreased albedo, since ozone strongly absorbs the incoming UV and visible solar radiation. For high ozone concentrations, surface temperatures drop by up to 8 K due to a change in energy balance. In the upper and middle atmosphere, temperatures increased by up to 60 K upon introducing ozone. The resulting increase in thermal flux balances the

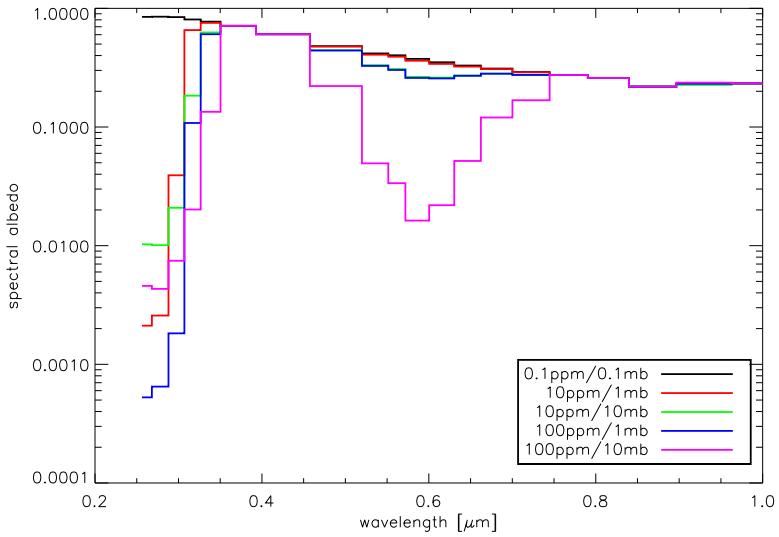

Figure 12: Effect of ozone on spectral albedo.

radiative forcing of UV absorption and leads to the observed surface cooling at high ozone concentrations.

As a consequence of the stratospheric warming, the cloud forming region is reduced. In the case of a thick ozone layer (comparable to or larger than the terrestrial ozone layer), cloud formation is inhibited completely.

For large ozone columns, convection is inhibited. Instead model atmospheres are fully radiative due to a strong reduction of incoming solar flux in the lower atmosphere. This probably decreases the vertical transport.

Upon increasing the ozone content in the model atmospheres, stratospheric water content strongly increased, due to a change in thermal structure and a change in cold trap location. Compared to zero-ozone simulations, water concentrations increased by up to two orders of magnitudes. This is important for assessing possible atmospheric water loss on early Mars, but could be a self-limiting effect due to enhanced catalytic HO_x cycles that destroy ozone.

Future work aims at performing fully coupled climate-chemistry simulations of early Mars as well as carbon dioxide-dominated atmospheres near the outer boundary of the habitable zone.

Acknowledgements

This study has received financial support from the French State in the frame of the "Investments for the future" Programme IdEx Bordeaux, reference ANR-10-IDEX-03-02. This work has been partly supported by the Postdoc Program "Atmospheric dynamics and Photochemistry of Super Earth planets" of the Helmholtz Gemeinschaft

(HGF). We thank the two anonymous reviewers for their positive and constructive feedback.

References

A. Borysow and L. Frommhold. Collision-induced rototranslational absorption spectra of N2-N2 pairs for temperatures from 50 to 300 K. *Astrophys. J.*, 311:1043–1057, December 1986. doi: 10.1086/164841.

K. Caldeira and J. F. Kasting. The life span of the biosphere revisited. *Nature*, 360: 721–723, December 1992. doi: 10.1038/360721a0.

E. Chassefière and F. Leblanc. Mars atmospheric escape and evolution; interaction with the solar wind. *Planet. Space Science*, 52:1039–1058, September 2004. doi: 10.1016/j.pss.2004.07.002.

S. Clough, F. Kneizys, and R. Davies. Line Shape and the Water Vapor Continuum. *Atm. Research*, 23:229–241, July 1989.

A. Colaprete and O. B. Toon. Carbon dioxide clouds in an early dense Martian atmosphere. *J. Geophys. Res.*, 108:6–1, April 2003. doi: 10.1029/2002JE001967.

P. J. Crutzen. The influence of nitrogen oxides on the atmospheric ozone content. *Quart. J. Royal Meteor. Soc.*, 96:320–325, April 1970. doi: 10.1002/qj.49709640815.

D. J. Des Marais, M. O. Harwit, K. W. Jucks, J. F. Kasting, D. N. C. Lin, J. I. Lunine, J. Schneider, S. Seager, W. A. Traub, and N. J. Woolf. Remote Sensing of Planetary Properties and Biosignatures on Extrasolar Terrestrial Planets. *Astrobiology*, 2:153–181, June 2002. doi: 10.1089/15311070260192246.

S. Domagal-Goldman and V. Meadows. Abiotic buildup of ozone. *ASP Conference Series*, 430:152, 2010.

S. D. Domagal-Goldman, A. Segura, M. W. Claire, T. D. Robinson, and V. S. Meadows. Abiotic Ozone and Oxygen in Atmospheres Similar to Prebiotic Earth. *Astrophys. J.*, 792:90, September 2014. doi: 10.1088/0004-637X/792/2/90.

J. Farquhar, J. Savarino, T. L. Jackson, and M. H. Thiemens. Evidence of atmospheric sulphur in the martian regolith from sulphur isotopes in meteorites. *Nature*, 404: 50–52, March 2000.

F. Forget and R. T. Pierrehumbert. Warming Early Mars with Carbon Dioxide Clouds That Scatter Infrared Radiation. *Science*, 278:1273–1276, November 1997.

F. Forget, R. Wordsworth, E. Millour, J.-B. Madeleine, L. Kerber, J. Leconte, E. Marcq, and R. M. Haberle. 3D modelling of the early martian climate under a denser CO_2 atmosphere: Temperatures and CO_2 ice clouds. *Icarus*, 222:81–99, January 2013. doi: 10.1016/j.icarus.2012.10.019.

J. L. Fox and A. Hać. Isotope fractionation in the photochemical escape of O from Mars. *Icarus*, 208:176–191, July 2010. doi: 10.1016/j.icarus.2010.01.019.

C. Gillmann, P. Lognonné, and M. Moreira. Volatiles in the atmosphere of Mars: The effects of volcanism and escape constrained by isotopic data. *Earth Plan. Science Letters*, 303:299–309, March 2011. doi: 10.1016/j.epsl.2011.01.009.

D. L. Glandorf, A. Colaprete, M. A. Tolbert, and O. B. Toon. CO_2 Snow on Mars and Early Earth: Experimental Constraints. *Icarus*, 160:66–72, November 2002. doi: 10.1006/icar.2002.6953.

C. Goldblatt, M. W. Claire, T. M. Lenton, A. J. Matthews, A. J. Watson, and K. J. Zahnle. Nitrogen-enhanced greenhouse warming on early Earth. *Nature Geoscience*, 2:891–896, December 2009. doi: 10.1038/ngeo692.

D. O. Gough. Solar interior structure and luminosity variations. *Solar Physics*, 74: 21–34, November 1981. doi: 10.1007/BF00151270.

J. L. Grenfell, J.-M. Grießmeier, B. Patzer, H. Rauer, A. Segura, A. Stadelmann, B. Stracke, R. Titz, and P. Von Paris. Biomarker Response to Galactic Cosmic Ray-Induced NO_x And The Methane Greenhouse Effect in The Atmosphere of An Earth-Like Planet Orbiting An M Dwarf Star. *Astrobiology*, 7:208–221, February 2007a. doi: 10.1089/ast.2006.0129.

J. L. Grenfell, B. Stracke, P. von Paris, B. Patzer, R. Titz, A. Segura, and H. Rauer. The response of atmospheric chemistry on earthlike planets around F, G and K Stars to small variations in orbital distance. *Planet. Space Science*, 55:661–671, April 2007b. doi: 10.1016/j.pss.2006.09.002.

J. L. Grenfell, S. Gebauer, P. von Paris, M. Godolt, P. Hedelt, A. B. C. Patzer, B. Stracke, and H. Rauer. Sensitivity of biomarkers to changes in chemical emissions in the Earth's Proterozoic atmosphere. *Icarus*, 211:81–88, January 2011. doi: 10.1016/j.icarus.2010.09.015.

J. L. Grenfell, S. Gebauer, M. Godolt, K. Palczynski, H. Rauer, J. Stock, P. von Paris, R. Lehmann, and F. Selsis. Potential Biosignatures in Super-Earth Atmospheres II. Photochemical Responses. *Astrobiology*, 13:415–438, May 2013. doi: 10.1089/ast.2012.0926.

J. L. Grenfell, S. Gebauer, P. v. Paris, M. Godolt, and H. Rauer. Sensitivity of biosignatures on Earth-like planets orbiting in the habitable zone of cool M-dwarf Stars to varying stellar UV radiation and surface biomass emissions. *Planet. Space Science*, 98:66–76, August 2014. doi: 10.1016/j.pss.2013.10.006.

M. Grott, A. Morschhauser, D. Breuer, and E. Hauber. Volcanic outgassing of CO_2 and H_2O on Mars. *Earth Plan. Science Letters*, 308:391–400, August 2011. doi: 10.1016/j.epsl.2011.06.014.

C. Gueymard. The sun's total and spectral irradiance for solar energy applications and solar radiation models. *Solar Energy*, 76:423–453, 2004.

I. Halevy and J. W. Head, III. Episodic warming of early Mars by punctuated volcanism. *Nature Geoscience*, 7:865–868, December 2014. doi: 10.1038/ngeo2293.

I. Halevy, M. T. Zuber, and D. P. Schrag. A Sulfur Dioxide Climate Feedback on Early Mars. *Science*, 318:1903–, December 2007. doi: 10.1126/science.1147039.

I. Halevy, R. T. Pierrehumbert, and D. P. Schrag. Radiative transfer in CO_2-rich paleoatmospheres. *J. Geophys. Res.*, 114:18112, September 2009. doi: 10.1029/2009JD011915.

P. Hedelt, P. von Paris, M. Godolt, S. Gebauer, J. L. Grenfell, H. Rauer, F. Schreier, F. Selsis, and T. Trautmann. Spectral features of Earth-like planets and their detectability at different orbital distances around F, G, and K-type stars. *Astron. Astrophys.*, 553:A9, May 2013. doi: 10.1051/0004-6361/201117723.

R. Hu, S. Seager, and W. Bains. Photochemistry in Terrestrial Exoplanet Atmospheres. I. Photochemistry Model and Benchmark Cases. *Astrophys. J.*, 761:166, December 2012. doi: 10.1088/0004-637X/761/2/166.

P. G. J. Irwin, J. K. Barstow, N. E. Bowles, L. N. Fletcher, S. Aigrain, and J.-M. Lee. The transit spectra of Earth and Jupiter. *Icarus*, 242:172–187, November 2014. doi: 10.1016/j.icarus.2014.08.005.

C. H. Jackman, J. E. Frederick, and R. S. Stolarski. Production of odd nitrogen in the stratosphere and mesosphere - An intercomparison of source strengths. *J. Geophys. Res.*, 85:7495–7505, December 1980. doi: 10.1029/JC085iC12p07495.

B. M. Jakosky and R. J. Phillips. Mars' volatile and climate history. *Nature*, 412: 237–244, July 2001.

S. S. Johnson, M. A. Mischna, T. L. Grove, and M. T. Zuber. Sulfur-induced greenhouse warming on early Mars. *J. Geophys. Res.*, 113:8005, August 2008. doi: 10.1029/2007JE002962.

L. Kaltenegger and W. A. Traub. Transits of Earth-like Planets. *Astrophys. J.*, 698: 519–527, June 2009. doi: 10.1088/0004-637X/698/1/519.

L. Kaltenegger, W. A. Traub, and K. W. Jucks. Spectral Evolution of an Earth-like Planet. *Astrophys. J.*, 658:598–616, March 2007. doi: 10.1086/510996.

L. Kaltenegger, A. Segura, and S. Mohanty. Model Spectra of the First Potentially Habitable Super-Earth Gl581d. *Astrophys. J.*, 733:35, May 2011. doi: 10.1088/0004-637X/733/1/35.

J. F. Kasting. Theoretical constraints on oxygen and carbon dioxide concentrations in the Precambrian atmosphere. *Precambrian Research*, 34:205–229, February 1987.

J. F. Kasting. Runaway and moist greenhouse atmospheres and the evolution of earth and Venus. *Icarus*, 74:472–494, June 1988. doi: 10.1016/0019-1035(88)90116-9.

J. F. Kasting. CO_2 condensation and the climate of early Mars. *Icarus*, 94:1–13, November 1991. doi: 10.1016/0019-1035(91)90137-I.

J. F. Kasting, J. B. Pollack, and T. P. Ackerman. Response of earth's atmosphere to increases in solar flux and implications for loss of water from Venus. *Icarus*, 57: 335–355, March 1984a. doi: 10.1016/0019-1035(84)90122-2.

J. F. Kasting, J. B. Pollack, and D. Crisp. Effects of high CO_2 levels on surface temperature and atmospheric oxidation state of the early earth. *J. Atmospheric Chem.*, 1:403–428, 1984b.

J. F. Kasting, D. P. Whitmire, and R. T. Reynolds. Habitable Zones around Main Sequence Stars. *Icarus*, 101:108–128, January 1993. doi: 10.1006/icar.1993.1010.

H. H. Kieffer, T. Z. Martin, A. R. Peterfreund, B. M. Jakosky, E. D. Miner, and F. D. Palluconi. Thermal and albedo mapping of Mars during the Viking primary mission. *J. Geophys. Res.*, 82:4249–4291, September 1977. doi: 10.1029/JS082i028p04249.

E. S. Kite, J.-P. Williams, A. Lucas, and O. Aharonson. Low palaeopressure of the martian atmosphere estimated from the size distribution of ancient craters. *Nature Geoscience*, 7:335–339, May 2014. doi: 10.1038/ngeo2137.

D. Kitzmann, A. B. C. Patzer, P. von Paris, M. Godolt, and H. Rauer. Clouds in the atmospheres of extrasolar planets. III. Impact of low and high-level clouds on the reflection spectra of Earth-like planets. *Astron. Astrophys.*, 534:A63, October 2011. doi: 10.1051/0004-6361/201117375.

D. Kitzmann, A. B. C. Patzer, and H. Rauer. Clouds in the atmospheres of extrasolar planets. IV. On the scattering greenhouse effect of CO_2 ice particles: Numerical radiative transfer studies. *Astron. Astrophys.*, 557:A6, September 2013. doi: 10.1051/0004-6361/201220025.

Y. N. Kulikov, H. Lammer, H. I. M. Lichtenegger, N. Terada, I. Ribas, C. Kolb, D. Langmayr, R. Lundin, E. F. Guinan, S. Barabash, and H. K. Biernat. Atmospheric and water loss from early Venus. *Planet. Space Science*, 54:1425–1444, November 2006. doi: 10.1016/j.pss.2006.04.021.

M. Kunze, M. Godolt, U. Langematz, J. L. Grenfell, A. Hamann-Reinus, and H. Rauer. Investigating the early Earth faint young Sun problem with a general circulation model. *Planet. Space Science*, 98:77–92, August 2014. doi: 10.1016/j.pss.2013.09.011.

W. J. Lafferty, A. M. Solodov, A. Weber, W. B. Olson, and J.-M. Hartmann. Infrared collision-induced absorption by N_2 near 4.3μm for atmospheric applications: measurements and empirical modeling. *Applied Optics*, 35:5911–5917, October 1996. doi: 10.1364/AO.35.005911.

H. Lammer, E. Chassefière, Ö. Karatekin, A. Morschhauser, P. B. Niles, O. Mousis, P. Odert, U. V. Möstl, D. Breuer, V. Dehant, M. Grott, H. Gröller, E. Hauber, and L. B. S. Pham. Outgassing History and Escape of the Martian Atmosphere and

Water Inventory. *Space Science Rev.*, 174:113–154, January 2013. doi: 10.1007/s11214-012-9943-8.

J. Laskar, A. C. M. Correia, M. Gastineau, F. Joutel, B. Levrard, and P. Robutel. Long term evolution and chaotic diffusion of the insolation quantities of Mars. *Icarus*, 170:343–364, August 2004. doi: 10.1016/j.icarus.2004.04.005.

J. Lasue, N. Mangold, E. Hauber, S. Clifford, W. Feldman, O. Gasnault, C. Grima, S. Maurice, and O. Mousis. Quantitative Assessments of the Martian Hydrosphere. *Space Science Rev.*, 174:155–212, January 2013. doi: 10.1007/s11214-012-9946-5.

S. Lebonnois, E. Quémerais, F. Montmessin, F. Lefèvre, S. Perrier, J.-L. Bertaux, and F. Forget. Vertical distribution of ozone on Mars as measured by SPICAM/Mars Express using stellar occultations. *J. Geophys. Res.*, 111:E09S05, September 2006. doi: 10.1029/2005JE002643.

A. Léger, J. M. Mariotti, B. Mennesson, M. Ollivier, J. L. Puget, D. Rouan, and J. Schneider. Could We Search for Primitive Life on Extrasolar Planets in the Near Future? *Icarus*, 123:249–255, October 1996. doi: 10.1006/icar.1996.0155.

P. R. Mahaffy, C. R. Webster, J. C. Stern, A. E. Brunner, S. K. Atreya, P. G. Conrad, S. Domagal-Goldman, J. L. Eigenbrode, G. J. Flesch, L. E. Christensen, H. B. Franz, C. Freissinet, D. P. Glavin, J. P. Grotzinger, J. H. Jones, L. A. Leshin, C. Malespin, A. C. McAdam, D. W. Ming, R. Navarro-Gonzalez, P. B. Niles, T. Owen, A. A. Pavlov, A. Steele, M. G. Trainer, K. H. Williford, J. J. Wray, and aff14. The imprint of atmospheric evolution in the D/H of Hesperian clay minerals on Mars. *Science*, 347:412–414, January 2015. doi: 10.1126/science.1260291.

M. Manga, A. Patel, J. Dufek, and E. S. Kite. Wet surface and dense atmosphere on early Mars suggested by the bomb sag at Home Plate, Mars. *Geophys. Res. Letters*, 39:L01202, January 2012. doi: 10.1029/2011GL050192.

T. R. Marrero and E. A. Mason. Gaseous Diffusion Coefficients. *J. Physical and Chemical Reference Data*, 1:3–118, January 1972. doi: 10.1063/1.3253094.

S. T. Massie and D. M. Hunten. Stratospheric eddy diffusion coefficients from tracer data. *J. Geophys. Res.*, 86:9859–9868, October 1981. doi: 10.1029/JC086iC10p09859.

C. P. McKay and C. R. Stoker. The Early Environment and its Evolution on Mars: Implications for Life. *Reviews of Geophysics*, 27:189–214, 1989. doi: 10.1029/RG027i002p00189.

M. A. Mischna, J. F. Kasting, A. Pavlov, and R. Freedman. Influence of carbon dioxide clouds on early martian climate. *Icarus*, 145:546–554, June 2000. doi: 10.1006/icar.2000.6380.

M. A. Mischna, C. Lee, and M. Richardson. Development of a fast, accurate radiative transfer model for the Martian atmosphere, past and present. *Journal of Geophysical Research (Planets)*, 117:E10009, October 2012. doi: 10.1029/2012JE004110.

M. A. Mischna, V. Baker, R. Milliken, M. Richardson, and C. Lee. Effects of obliquity and water vapor/trace gas greenhouses in the early martian climate. *Journal of Geophysical Research (Planets)*, 118:560–576, March 2013. doi: 10.1002/jgre.20054.

E. J. Mlawer, S. J. Taubman, P. D. Brown, M. J. Iacono, and S. A. Clough. Radiative transfer for inhomogeneous atmospheres: RRTM, a validated correlated-k model for the longwave. *J. Geophys. Res.*, 102:16663–16682, July 1997. doi: 10.1029/97JD00237.

F. Montmessin, J.-L. Bertaux, F. Lefèvre, E. Marcq, D. Belyaev, J.-C. Gérard, O. Korablev, A. Fedorova, V. Sarago, and A. C. Vandaele. A layer of ozone detected in the nightside upper atmosphere of Venus. *Icarus*, 216:82–85, November 2011. doi: 10.1016/j.icarus.2011.08.010.

H. Nair, M. Allen, A. D. Anbar, Y. L. Yung, and R. T. Clancy. A photochemical model of the martian atmosphere. *Icarus*, 111:124–150, September 1994. doi: 10.1006/icar.1994.1137.

R. H. Norton and C. P. Rinsland. ATMOS data processing and science analysis methods. *Applied Optics*, 30:389–400, February 1991. doi: 10.1364/AO.30.000389.

R. J. Phillips, M. T. Zuber, S. C. Solomon, M. P. Golombek, B. M. Jakosky, W. B. Banerdt, D. E. Smith, R. M. E. Williams, B. M. Hynek, O. Aharonson, and S. A. Hauck. Ancient Geodynamics and Global-Scale Hydrology on Mars. *Science*, 291:2587–2591, March 2001. doi: 10.1126/science.1058701.

R. T. Pierrehumbert and C. Erlick. On the Scattering Greenhouse Effect of CO_2 Ice Clouds. *J. Atmosph. Sciences*, 55:1897–1903, May 1998.

S. E. Postawko and W. R. Kuhn. Effect of the greenhouse gases (CO2, H2O, SO2) on Martian paleoclimate. *J. Geophys. Res.*, 91:431, March 1986. doi: 10.1029/JB091iB04p0D431.

R. M. Ramirez, R. Kopparapu, M. E. Zugger, T. D. Robinson, R. Freedman, and J. F. Kasting. Warming early Mars with CO_2 and H_2. *Nature Geoscience*, 7:59–63, January 2014. doi: 10.1038/ngeo2000.

H. Rauer, S. Gebauer, P. von Paris, J. Cabrera, M. Godolt, J. L. Grenfell, A. Belu, F. Selsis, P. Hedelt, and F. Schreier. Potential Biosignatures in Super-Earths Atmospheres I. Spectral appearance of super-Earths around M dwarfs. *Astron. Astrophys.*, 529:A8, May 2011. doi: 10.1051/0004-6361/201014368.

I. Ribas, E. F. Guinan, M. Güdel, and M. Audard. Evolution of the Solar Activity over Time and Effects on Planetary Atmospheres. I. High-Energy Irradiances (1-1700 Å). *Astrophys. J.*, 622:680–694, March 2005. doi: 10.1086/427977.

E. Roeckner, R. Brokopf, M. Esch, M. Giorgetta, S. Hagemann, L. Kornblueh, E. Manzini, U. Schlese, and U. Schulzweida. Sensitivity of Simulated Climate to Horizontal and Vertical Resolution in the ECHAM5 Atmosphere Model. *J. Climate*, 19:3771, 2006. doi: 10.1175/JCLI3824.1.

L. S. Rothman, I. E. Gordon, A. Barbe, D. C. Benner, P. F. Bernath, M. Birk, V. Boudon, L. R. Brown, A. Campargue, J.-P. Champion, K. Chance, L. H. Coudert, V. Dana, V. M. Devi, S. Fally, J.-M. Flaud, R. R. Gamache, A. Goldman, D. Jacquemart, I. Kleiner, N. Lacome, W. J. Lafferty, J.-Y. Mandin, S. T. Massie, S. N. Mikhailenko, C. E. Miller, N. Moazzen-Ahmadi, O. V. Naumenko, A. V. Nikitin, J. Orphal, V. I. Perevalov, A. Perrin, A. Predoi-Cross, C. P. Rinsland, M. Rotger, M. Šimečková, M. A. H. Smith, K. Sung, S. A. Tashkun, J. Tennyson, R. A. Toth, A. C. Vandaele, and J. Vander Auwera. The HITRAN 2008 molecular spectroscopic database. *J. Quant. Spect. Rad. Trans.*, 110:533–572, June 2009. doi: 10.1016/j.jqsrt.2009.02.013.

T. L. Schindler and J. F. Kasting. Synthetic Spectra of Simulated Terrestrial Atmospheres Containing Possible Biomarker Gases. *Icarus*, 145:262–271, May 2000. doi: 10.1006/icar.2000.6340.

F. Schreier and U. Böttger. MIRART, a line-by-line code for infrared atmospheric radiation computations including derivatives. *Atmospheric and Oceanic Optics*, 16: 262–268, 2003.

F. Schreier and B. Schimpf. A new efficient line-by-line code for high resolution atmospheric radiation computations incl. derivatives. In W.L. Smith and Y. Timofeyev, editors, *IRS 2000: Current Problems in Atmospheric Radiation*, Current Problems in Atmospheric Radiation. A. Deepak, 2001.

A. Segura and R. Navarro-González. Nitrogen fixation on early Mars by volcanic lightning and other sources. *Geophys. Res. Letters*, 32:L5203, March 2005. doi: 10.1029/2004GL021910.

A. Segura, K. Krelove, J. F. Kasting, D. Sommerlatt, V. Meadows, D. Crisp, M. Cohen, and E. Mlawer. Ozone Concentrations and Ultraviolet Fluxes on Earth-Like Planets Around Other Stars. *Astrobiology*, 3:689–708, December 2003. doi: 10.1089/153110703322736024.

A. Segura, J. F. Kasting, V. Meadows, M. Cohen, J. Scalo, D. Crisp, R. A. H. Butler, and G. Tinetti. Biosignatures from Earth-Like Planets Around M Dwarfs. *Astrobiology*, 5:706–725, December 2005. doi: 10.1089/ast.2005.5.706.

A. Segura, V. S. Meadows, J. F. Kasting, D. Crisp, and M. Cohen. Abiotic formation of O_2 and O_3 in high-CO_2 terrestrial atmospheres. *Astron. Astrophys.*, 472:665–679, 2007.

T. L. Segura, O. B. Toon, and A. Colaprete. Modeling the environmental effects of moderate-sized impacts on Mars. *J. Geophys. Res.*, 113:E11007, November 2008. doi: 10.1029/2008JE003147.

F. Selsis. Review: Physics of Planets I: Darwin and the Atmospheres of Terrestrial Planets. *ESA Special Publication*, 451:133, 2000.

F. Selsis, D. Despois, and J.-P. Parisot. Signature of life on exoplanets: Can Darwin produce false positive detections? *Astron. Astrophys.*, 388:985–1003, June 2002. doi: 10.1051/0004-6361:20020527.

B. Stevens, M. Giorgetta, M. Esch, T. Mauritsen, T. Crueger, S. Rast, M. Salzmann, H. Schmidt, J. Bader, K. Block, R. Brokopf, I. Fast, S. Kinne, L. Kornblueh, U. Lohmann, R. Pincus, T. Reichler, and E. Roeckner. Atmospheric component of the MPI-M Earth System Model: ECHAM6. *J. of Adv. in Modeling Earth Systems*, 5:146–172, June 2013. doi: 10.1002/jame.20015.

J. W. Stock, C. S. Boxe, R. Lehmann, J. L. Grenfell, A. B. C. Patzer, H. Rauer, and Y. L. Yung. Chemical pathway analysis of the Martian atmosphere: CO2-formation pathways. *Icarus*, 219:13–24, May 2012a. doi: 10.1016/j.icarus.2012.02.010.

J. W. Stock, J. L. Grenfell, R. Lehmann, A. B. C. Patzer, and H. Rauer. Chemical pathway analysis of the lower Martian atmosphere: The CO2 stability problem. *Planet. Space Science*, 68:18–24, August 2012b. doi: 10.1016/j.pss.2011.03.002.

F. Tian, M. W. Claire, J. D. Haqq-Misra, M. Smith, D. C. Crisp, D. Catling, K. Zahnle, and J. F. Kasting. Photochemical and climate consequences of sulfur outgassing on early Mars. *Earth Plan. Science Letters*, 295:412–418, July 2010. doi: 10.1016/j.epsl.2010.04.016.

F. Tian, K. France, J. L. Linsky, P. J. D. Mauas, and M. C. Vieytes. High stellar FUV/NUV ratio and oxygen contents in the atmospheres of potentially habitable planets. *Earth Plan. Science Letters*, 385:22–27, January 2014. doi: 10.1016/j.epsl.2013.10.024.

O. B. Toon, C. P. McKay, T. P. Ackerman, and K. Santhanam. Rapid calculation of radiative heating rates and photodissociation rates in inhomogeneous multiple scattering atmospheres. *J. Geophys. Res.*, 94:16287–16301, 1989.

P. von Paris, H. Rauer, J. L. Grenfell, B. Patzer, P. Hedelt, B. Stracke, T. Trautmann, and F. Schreier. Warming the early Earth - CO_2 reconsidered. *Planet. Space Science*, 56:1244–1259, October 2008. doi: 10.1016/j.pss.2008.04.008.

P. von Paris, S. Gebauer, M. Godolt, J. L. Grenfell, P. Hedelt, D. Kitzmann, A. B. C. Patzer, H. Rauer, and B. Stracke. The extrasolar planet GL 581 d: A potentially habitable planet? *Astron. Astrophys.*, 522:A23, November 2010. doi: 10.1051/0004-6361/201015329.

P. von Paris, J. L. Grenfell, P. Hedelt, H. Rauer, F. Selsis, and B. Stracke. Atmospheric constraints for the CO2 partial pressure on terrestrial planets near the outer edge of the habitable zone. *Astron. Astrophys.*, 549:A94, January 2013a. doi: 10.1051/0004-6361/201016058.

P. von Paris, J. L. Grenfell, H. Rauer, and J. W. Stock. N_2-associated surface warming on early Mars. *Planet. Space Science*, 82:149–154, July 2013b. doi: 10.1016/j.pss.2013.04.009.

P. von Paris, P. Hedelt, F. Selsis, F. Schreier, and T. Trautmann. Characterization of potentially habitable planets: Retrieval of atmospheric and planetary properties from emission spectra. *Astron. Astrophys.*, 551:A120, March 2013c. doi: 10.1051/0004-6361/201220009.

P. von Paris, F. Selsis, D. Kitzmann, and H. Rauer. The dependence of the ice-albedo feedback on atmospheric properties. *Astrobiology*, 13:899–909, October 2013d. doi: 10.1089/ast.2013.0993.

R. Wordsworth and R. Pierrehumbert. Abiotic Oxygen-dominated Atmospheres on Terrestrial Habitable Zone Planets. *Astrophys. J. Letters*, 785:L20, April 2014. doi: 10.1088/2041-8205/785/2/L20.

R. Wordsworth, F. Forget, and V. Eymet. Infrared collision-induced and far-line absorption in dense CO_2 atmospheres. *Icarus*, 210:992–997, December 2010. doi: 10.1016/j.icarus.2010.06.010.

R. Wordsworth, F. Forget, E. Millour, J. Head, J.-B. Madeleine, and B. Charnay. Global modelling of the early Martian climate under a denser CO2 atmosphere: Water cycle and ice evolution. *Icarus*, 222(1):1–19, January 2013. doi: 10.1016/j.icarus.2012.09.036.

Y. L. Yung and W. B. deMore. *Photochemistry of Planetary Atmospheres*. Oxford University Press, 1999.

Y. L. Yung, H. Nair, and M. F. Gerstell. NOTE: CO_2 Greenhouse in the Early Martian Atmosphere: SO_2 Inhibits Condensation. *Icarus*, 130:222–224, November 1997. doi: 10.1006/icar.1997.5808.

K. Zahnle. Play it again, SAM. *Science*, 347:370–371, January 2015. doi: 10.1126/science.aaa3687.